# Binary neutron star formation and the origin of GW170817

K. Belczynski<sup>1\*</sup>, T. Bulik<sup>2</sup>, A.Olejak<sup>2</sup>, M. Chruslinska<sup>3</sup>, N. Singh<sup>2</sup>, N. Pol<sup>4</sup>, L. Zdunik<sup>1</sup>, R. O'Shaughnessy<sup>5</sup>, M. McLaughlin<sup>4</sup>, D. Lorimer<sup>4</sup>, O. Korobkin<sup>6</sup>, E.P.J. van den Heuvel<sup>7</sup>, M.B. Davies<sup>8</sup>, and D. Holz<sup>9</sup>

- <sup>1</sup> Nicolaus Copernicus Astronomical Center, Polish Academy of Sciences, ul. Bartycka 18, 00-716 Warsaw, Poland
- Astronomical Observatory, Warsaw University, Ujazdowskie 4, 00-478 Warsaw, Poland
- Department of Astrophysics/IMAPP, Radboud University, P.O. Box 9010, 6500 GL Nijmegen, The Netherlands
- Department of Physics and Astronomy, West Virginia University, Morgantown, West Virginia 26506, USA; Center for Gravitational Waves and Cosmology, West Virginia University, Chestnut Ridge Research Building, Morgantown, West Virginia 26505, USA
- Center for Computational Relativity and Gravitation, Rochester Institute of Technology, Rochester, New York 14623, USA
- <sup>6</sup> Center for Theoretical Astrophysics, Los Alamos National Laboratory, Los Alamos, NM 87545, USA
- Astronomical Institute Anton Pannekoek, University of Amsterdam, PO Box 94249, 1090 GE Amsterdam, the Netherlands
- <sup>8</sup> Lund Observatory, Box 43, SE-221 00 Lund, Sweden
- <sup>9</sup> Enrico Fermi Institute, Department of Physics, Department of Astronomy and Astrophysics, and Kavli Institute for Cosmological Physics, University of Chicago, Chicago, IL 60637, USA

Received Dec 25, 2018; accepted ???

#### **ABSTRACT**

The first neutron star-neutron star merger (NS-NS: GW170817) was detected in gravitational waves by LIGO/Virgo in a galaxy in which the majority of star formation was taking place a long time ago ( $\sim 11$  Gyr). Based on this single event, LIGO/Virgo estimated that local cosmic NS-NS merger rate is 110–3840 Gpc<sup>-3</sup> yr<sup>-1</sup> (90% confidence range). Only some extreme evolutionary models (with very small NS natal kicks and very high common envelope efficiency) can generate NS-NS merger rates in old host galaxies consistent with the LIGO/Virgo estimate ( $\gtrsim 100$  Gpc<sup>-3</sup> yr<sup>-1</sup>). However, we show that these models generate rates exceeding empirical Galactic NS-NS merger rates based on the large population of Milky Way NS-NS binaries.

Typically, current evolutionary models produce NS-NS merger rates that are consistent with the Milky Way empirical rates ( $\sim 10$ –200 Myr<sup>-1</sup>). However, these models generate local ( $z \approx 0$ ) cosmic NS-NS merger rate in old host galaxies ( $\sim 1$ –70 Gpc<sup>-3</sup> yr<sup>-1</sup>) that are below the LIGO/Virgo estimate. The reason behind this tension is the predicted delay time distribution between star formation and NS-NS mergers that favors short delays.

Evolutionary models produce a generic steep power-law ( $\propto t^{-1}$ ) NS-NS delay time distribution. This limits NS-NS merger rates in old host galaxies. However, we show that such distribution is consistent with observations of Galactic NS-NS binaries; 50% of which show very long merger times (much longer than Hubble time). Once model distributions are convolved with continuous prolonged (10 Gyr) star formation in the Galactic disk, then  $\sim 20-70\%$  (depending on a model) of the predicted NS-NS population has very long current Galactic merger times (> 30 Gyr). Although NS-NS binaries are formed predominantly with short delay times, many of short delay time systems merge and do not make it to the present, while long delay time systems survive and contribute to the current Galactic NS-NS population.

This study highlights the tension between the current evolutionary predictions and the observation of the first NS-NS merger in an old host galaxy. It is crucial to understand that models need to explain not only the LIGO/Virgo rate estimate, but also the merger site.

**Key words.** Stars: massive – Neutron-star physics – Gravitational waves

# 1. Introduction

LIGO/Virgo have discovered the first NS-NS merger through gravitational waves and estimated the local cosmic NS-NS merger rate: 110–3840 Gpc $^{-3}$  yr $^{-1}$  (90% credible range with peak probability of  $\sim 1000$  Gpc $^{-3}$  yr $^{-1}$ ; Abbott et al. (2017a); The LIGO Scientific Collaboration & the Virgo Collaboration (2018)). The merger was quickly localized in a nearby host galaxy 40 Mpc away (Abbott et al. 2017b). In this galaxy, NGC 4993, star formation peaked  $\sim 11$  Gyr ago (at level  $\sim 10~M_{\odot}~yr^{-1}$ ) and then was exponentially declining, leading to a very low current star formation rate ( $\sim 0.01~M_{\odot}~yr^{-1}$ ). The total mass formed in stars was estimated at  $7.9\times10^{10}~M_{\odot}$ . In particular, the 50% of stars formed by 11.2 Gyr ago, while 90% of stars formed by 6.8 Gyr ago (Blanchard et al. 2017). Stars in NGC

4993 appear to have near solar chemical composition (Blanchard et al. 2017; Troja et al. 2017; Palmese et al. 2017).

It was reported that the central parts of NGC 4993 appear to have shell and dust structures that may be indicative of a recent minor galaxy merger or mergers. However, Troja et al. (2017), based on available UV information, concludes that there is no ongoing star formation at the NS-NS merger site and argue against young (< 2 Gyr) stellar populations in NGC 4993 based on optical spectral analysis. Palmese et al. (2017) use Dark Energy Camera imaging along with detailed spectral analysis of available data to estimate the star formation rate specific to a potential recent minor merger and finds little to no ongoing star formation and conclude that GW170817 is not likely associated with recent star formation. Finally, Blanchard et al. (2017) present detailed spectral, photometric and image analysis to calculate the star formation history in NGC 4993. In fact, this

<sup>\*</sup> chrisbelczynski@gmail.com

analysis reveals some extra component in the recent star formation history indicative of a minor merger (see the flattening at t=0.1-1 Gyr ago in their exponentially declining SFR; their Fig.3 left-bottom panel). However, this recent episode provides only a small fraction of the overall stellar mass in NGC 4993. For example, the entire episode (t=0.1-1 Gyr ago) provides only  $\sim 0.3 \times 10^9 \ M_{\odot}$  (0.4% of total mass formed in stars), while the most recent part of extra star formation (t=0.1-0.3 Gyr ago) provides only  $\sim 0.3 \times 10^8 \ M_{\odot}$  (0.04% of total mass formed in stars; these values can be read of Fig.3 of Blanchard et al. (2017)).

The discovery of GW170817, accompanied by an unusual weak/offaxis short gamma-ray burst (GRB), and by a strong kilonova IR/optical counterpart, and long-lived X-ray afterglow triggered a search for similar events in the existing data. Troja et al. (2018) have identified one such event: GRB 150101B at redshift z = 0.1341. This event is a low-luminosity short GRB, with strong optical emission and long-lived X-ray emission estimated to be viewed at an angle of 13 degrees. At this distance ( $\sim 600$  Mpc) a NS-NS merger is undetectable by LIGO/Virgo (even at their design sensitivity). However, the physical properties seem to by symptomatic of a NS-NS merger, or at least similar to the one observed in NGC 4993. GRB 150101B is located within its host galaxy 7.3 kpc from its center. The most interesting fact is that this is an early type galaxy with mean stellar age of  $2^{+6}_{-1}$  Gyr typical of elliptical galaxies (see Fig.5 of Troja et al. (2018)).

Isolated binary evolution in galactic fields and dynamical evolution in globular or nuclear clusters are the main formation channels for NS-NS binaries. For example, in the Milky Way there are 18 known NS-NS systems; 16 of which are found in the Galactic disk/field, and 2 in Galactic globular clusters (see Tab. 1). The GW170817 projected distance from the center of NGC 4993 is 2.1 kpc: within the galaxy half-light radius. Also there is no visible globular cluster in the vicinity of the merger (Blanchard et al. 2017; Troja et al. 2017; Palmese et al. 2017). Evolutionary predictions indicate that binary evolution dominates the formation rate of NS-NS mergers at late times after star formation in galaxies like NGC 4993, over globular and nuclear cluster rates by 2–3 orders of magnitude (Belczynski et al. 2018).

In this study, we will focus on the isolated binary evolution channel in the context of the formation of GW170817 in NGC 4993. Current evolutionary predictions based on population synthesis calculations typically generate local cosmic ( $z \approx 0$ ) NS-NS merger rates at the level  $\sim 100 \, \rm Gpc^{-3} \, yr^{-1}$ . However, if several not fully constrained evolutionary parameters (e.g., NS natal kicks, common envelope efficiency, Roche lobe overflow treatment) are pushed in favor of NS-NS formation, the merger rates can reach  $\sim 500 \, \mathrm{Gpc^{-3} \, yr^{-1}}$  (Chruslinska et al. 2018; Kruckow et al. 2018; Vigna-Gómez et al. 2018; Mapelli & Giacobbo 2018)<sup>1</sup>. This is consistent with the LIGO/Virgo lowend of 90% confidence range of the NS-NS merger rate (110– 3840 Gpc<sup>-3</sup> yr<sup>-1</sup>). It may seem like there is apparently no tension between the LIGO/Virgo observation and these theoretical predictions. However, the merger rate of NS-NS systems is directly proportional to star forming mass for isolated binary evolution and evolutionary predictions show a generic delay time

distribution ( $\propto t^{-1}$ ) that favors short delay times. This indicates that NS-NS mergers are more likely in host galaxies with ongoing or recent star formation. If we take into account the fact that locally only 1/3 of galaxies are ellipticals (Conselice et al. 2016) then predicted isolated binary evolution rates drop from  $\sim 500~\rm Gpc^{-3}~\rm yr^{-1}$  to  $\sim 170~\rm Gpc^{-3}~\rm yr^{-1}$ , which is then only marginally consistent with the LIGO/Virgo empirical estimate. Note that such estimate completely ignores the fact that NS-NS merger rate depends strongly on delay time distribution and thus star formation history in a given type of host galaxy. This factor can be easily assessed for elliptical hosts. Elliptical galaxies typically formed the majority of stars 1-10 Gyr ago (Gallazzi et al. 2006). There is an expectation (confirmed by evolutionary calculations; e.g., see Sec. 4.1) that NS-NS binaries typically begin merging ~ 100 Myr after star formation (stellar evolution takes several tens of Myr to form NSs out of massive stars). If the above is taken into account, then the current NS-NS merger rate in ellipticals decreases by 1-2 orders of magnitude with respect to the above optimistic estimate. This means that the current local cosmic merger rate in ellipticals predicted by evolutionary calculations is at most  $\sim 1.7-17$  Gpc<sup>-3</sup> yr<sup>-1</sup>. If the LIGO/Virgo single observation is to be trusted (note that small number statistics/Poisson errors were taken into account in the LIGO/Virgo rate estimate) then there is a tension between evolutionary predictions and the LIGO/Virgo observation of GW170817. In other words, current evolutionary predictions cannot explain formation of NS-NS mergers in old host galaxies at such rates that it would warrant detection at the current LIGO/Virgo sensitivity (~ 70 Mpc; Abbott et al. (2017a)), as one expects a merger in elliptical galaxy to be detected every 50-500 years.

We can use the same line of reasoning to show that a potential minor galaxy merger in the recent past of NGC 4993 was not likely to produce a NS-NS merger through isolated binary evolution. Let's start with all elliptical galaxies in the local Universe; their entire star forming mass is predicted to produce a NS-NS merger rate of  $\sim 170 \, \mathrm{Gpc^{-3}} \, \mathrm{yr^{-1}}$  in optimistic evolutionary models that assume constant star formation. Let's put 1% of this star forming mass at such preferable times that all NS-NS mergers could be detected by the LIGO/Virgo. This way we circumnavigate the issue of long delays expected for elliptical host galaxies. Then the expected current merger rate is only  $\sim 1.7 \,\mathrm{Gpc^{-3}\ yr^{-1}}$ , and in clear tension with LIGO/Virgo empirical estimate. Note that for this exercise we assumed a rather large stellar mass of a minor merger (for NGC 4993 we estimated this mass to be only 0.04 – 0.4% of entire galaxy star forming mass) and we assumed that every elliptical in the LIGO/Virgo range went through such minor merger at the best preferable time so all NS-NS mergers could have been detected.

It seems like the steep delay time distribution is the major factor limiting NS-NS merger rates in old host galaxies in evolutionary models. In the following sections we will re-examine the issue of delay time distributions obtained in evolutionary models and compare them with available observations of Galactic NS-NS binaries. If models with steep delay time distributions do not reproduce the properties of Galactic NS-NS systems (their observed merger times and merger rates) then this will indicate a need for a major revision of models. However, if the models do reproduce the observed population of Galactic NS-NS binaries, then other options may need to be invoked to explain GW170817. For example, GW170817 was a significant statistical fluctuation, or this NS-NS merger was produced by other process than isolated binary evolution.

<sup>&</sup>lt;sup>1</sup> There is one exception to this general consensus. Apparently, simulations based on BPASS populations synthesis code (Eldridge et al. 2017) generate very large NS-NS merger rates: 1000–5000 Gpc<sup>-3</sup> yr<sup>-1</sup> if BPASS newly proposed NS natal kick prescription is applied (Bray & Eldridge 2018; Eldridge et al. 2018). However, note that such high rates are not consistent with empirical Galactic NS-NS merger rate estimates (see Sec. 5 for discussion).

Table 1. Galactic NS-NS binaries<sup>a</sup>

Name	type	$M_{\rm psr}^{\ \ b}$	$M_{\rm com}$	$P_{\mathrm{orb}}$	а	e	$t_{\rm mer}^{\ c}$	reference <sup>e</sup>
		$[M_{\odot}]$	$[ M_{\odot}]$	[day]	$[R_{\odot}]$		[Gyr]	
field:								
1) J1946+2052	recycled	1.25	1.25	0.076	1.028	0.06	0.042	[1]
2) J1757-1854	recycled	1.34	1.39	0.183	1.897	0.6	0.079	[2]
3) J0737-3039	young	1.338	1.249	0.102	1.261	0.088	0.085	[3,4,5]
4) B1913+16	recycled	1.440	1.389	0.323	2.801	0.617	0.301	[6,7]
5) J1906+0746	young	1.291	1.322	0.166	1.750	0.085	0.308	[8,9]
6) J1913+1102	recycled	1.64	1.25	0.206	2.090	0.08	0.473	[10,11]
7) J1756-2251	recycled	1.341	1.230	0.320	2.696	0.181	1.660	[12,13]
8) B1534+12	recycled	1.333	1.346	0.421	3.282	0.274	2.736	[14]
9) J1829+2456	recycled	1.295	1.295	1.176	6.436	0.139	55.36	[15]
10) J1411+2551	recycled	1.265	1.265	2.61	10.9	0.16	471.3	[16]
11) J0453+1559	recycled	1.559	1.174	4.072	15.0	0.113	1,452	[17]
12) J1811-1736	recycled	1.285	1.285	18.779	40.7	0.828	1,794	[18]
13) J1518+4904	recycled	1.359	1.359	8.634	24.7	0.249	8,853	[19]
14) J1755-2550	young	1.3	1.3	9.696	26.3	0.089	15,917	[20,21]
15) J1753-2240	recycled	1.3	1.3	13.638	33.0	0.304	28,646	[22]
16) J1930-1852	recycled	1.295	1.295	45.060	73.1	0.399	531,294	[23]
globular clusters:								
17) B2127+11C	recycled	1.358	1.354	0.335	2.830	0.681	0.217	[24,25]
18) J1807-2500B <sup>d</sup>	recycled	1.366	1.206	9.957	26.7	0.747	1,044	[26]

#### Notes.

## 2. Binary evolutionary models

Binary evolution calculations are performed with the upgraded population synthesis code StarTrack (Belczynski et al. 2002, 2008). The existing improvements relevant for massive star evolution include updates to the treatment of common envelope (CE) evolution (Xu & Li 2010; Dominik et al. 2012), the compact object masses produced by core collapse/supernovae (Fryer et al. 2012; Belczynski et al. 2012) with the effect of pair-instability pulsation supernovae and pair-instability supernovae (Woosley et al. 2007; Belczynski et al. 2016a), stellar binary initial conditions set by observations (Sana et al. 2012; de Mink & Belczynski 2015), and observationally constrained star formation and metallicity evolution over cosmic time (Madau & Dickinson 2014; Belczynski et al. 2016b). The code adopts by default the fallback-decreased natal kick prescription (Belczynski et al. 2017).

For our study we select fifteen evolutionary models (M10 and NN1–NN14) which differ significantly by some evolutionary assumptions important for massive star evolution. The model M10 is fully described by Belczynski et al. (2017). For model M10 standard evolutionary assumptions are adopted: standard NS/BH masses Fryer et al. (2012) with pair-instability pulsations and SNe, low-to-no BH natal kicks (set by fallback), high kicks for core-collapse (CC) NSs drawn from Maxwellian with

with 1-dimensional  $\sigma=265~\rm km~s^{-1}$  and modified by fallback, no natal kicks for electron-capture supernova (ECS) NS formation, 50% non-conservative RLOF, 10% Bondi-Hoyle rate accretion onto NS/BH in CE, no effects of rotation on stellar evolution<sup>2</sup>, initial binary parameters from Sana et al. (2012), and massive star winds Vink et al. (2001); Belczynski et al. (2010a) with LBV winds calibrated to produce BHs with maximum mass of 15  $\rm M_{\odot}$  at current Galactic disk metallicity ( $\rm Z=0.02$ :  $(dM/dt)_{\rm LBV}=1.5\times10^{-4}~\rm M_{\odot}~yr^{-1}$ ).

In model NN2 we assume high CC NS natal kicks with  $\sigma=265~{\rm km~s^{-1}}$  without any fallback effect. ECS NSs receive exactly the same natal kicks as CC NSs. During CE we assume that 100% of orbital energy is used to eject the envelope, and this corresponds to CE efficiency of  $\alpha_{\rm CE}=1.0$ . During nonconservative RLOF, 20% of donor mass transfer is accreted onto non-degenerate companion, while 80% of donor mass transfer is ejected from binary.

In model NN14, all the assumptions are the same as in model NN2, with one exception. We assume here that CC NS natal kicks are moderated by small amount of fallback expected even in NS formation (Fryer et al. 2012). All NS natal kicks are thus somewhat smaller than in model NN2.

<sup>&</sup>lt;sup>a</sup> All known Galactic systems

<sup>&</sup>lt;sup>b</sup> If only total mass is reported in literature, we use  $M_{psr}=M_{com}=0.5M_{tot}$ .

<sup>&</sup>lt;sup>c</sup> Current time to merger estimated from NS masses and currently measured orbital parameters: a and e.

<sup>&</sup>lt;sup>d</sup> This may be potentially a NS-WD system: https://www3.mpifr-bonn.mpg.de/staff/pfreire/NS\_masses.html.

<sup>&</sup>lt;sup>e</sup> [1]: Stovall et al. (2018); [2]: Cameron et al. (2018); [3]: Kramer et al. (2006); [4]: Breton et al. (2008); [5]: Ferdman et al. (2013); [6]: Hulse & Taylor (1975); [7]: Weisberg et al. (2010); [8]: Lorimer et al. (2006); [9]: van Leeuwen et al. (2015); [10]: Lazarus et al. (2016); [11]: Ferdman & PALFA Collaboration (2018); [12]: Faulkner et al. (2005); [13]: Ferdman et al. (2014); [14]: Fonseca et al. (2014); [15]: Champion et al. (2004); [16]: Martinez et al. (2017); [17]: Martinez et al. (2015); [18]: Corongiu et al. (2007); [19]: Janssen et al. (2008); [20]: Ng et al. (2015); [21]: Ng et al. (2018); [22]: Keith et al. (2009); [23]: Swiggum et al. (2015); [24]: Anderson et al. (1990); [25]: Jacoby et al. (2006); [26]: Lynch et al. (2012).

<sup>&</sup>lt;sup>2</sup> Binary component spins are followed (tides, magnetic braking and change of inertia). However, stellar rotation does not alter internal star properties (He/CO core mass).

In model NN3, all the assumptions are the same as in model NN14, with one exception. We assume here that ECS NSs receive different natal kicks than CC NSs. Natal kicks for ECS NSs in this model are assumed to be zero.

In models NN7 and NN8 we assume similar physics as in model NN2, but we introduce two modifications. CC NS natal kicks are drawn from the distribution with smaller kicks:  $\sigma = 133 \text{ km s}^{-1}$ . ECS NSs are assumed to receive different natal kicks than CC NSs: drawn from Maxwellian with 1-dimensional  $\sigma = 66 \text{ km s}^{-1}$  for model NN7, and with zero natal kicks for model NN8.

In model NN11 we use the same assumptions as in model NN2, however we lower significantly CC NS natal kicks to  $\sigma = 66 \, \mathrm{km \ s^{-1}}$ . Note that this applies to all NSs, as ECS natal kicks are treated the same way as the CC NS kicks.

In models NN9 and NN10 we assume similar physics as in model NN11, but we allow for different ECS NS natal kicks. ECS natal kicks are drawn from Maxwellian with 1-dimensional  $\sigma=33~{\rm km~s^{-1}}$  for model NN9, and with zero natal kicks for model NN10.

In models NN12 and NN4 we use the same assumptions as in models NN2 and NN11. However, we further lower CC NS natal kicks to  $\sigma=33~\rm km~s^{-1}$  for model NN12 and to  $\sigma=0~\rm km~s^{-1}$  (no natal kicks) for model NN4.

In model N13, we adopt same assumptions as in model NN4, with one modification of CE treatment: very high common envelope efficiency  $\alpha_{\rm CE}=10$ . Note that this model has not only the lowest possible NS natal kicks (like in NN4), but also most likely unrealistically high CE efficiency.

In models NN1, NN5 and NN6 we adopt Bray & Eldridge (2018) natal kicks for both ECS and CC NSs (they use the same prescription for CC and ECS NSs). The 3-dimensional natal kick magnitude is taken from

$$v_{\text{kick}} = \alpha (M_{\text{ejecta}}/M_{\text{remnant}}) + \beta,$$
 (1)

while the direction of natal kick is random. This prescription was adopted with specific natal kick parameters proposed by these authors:  $\alpha=100~{\rm km~s^{-1}}$  and  $\beta=-170~{\rm km~s^{-1}}$ ; note that this prescription produces almost zero NS natal kicks. Each of these three models differs only by one parameter, CE efficiency:  $\alpha_{\rm CE}=0.1,~1.0,~10$  for NN5, NN1 and NN6, respectively. All the rest of physical assumptions are the same as in model NN2.

For main sequence donors CE is assumed always to lead to binary component merger aborting binary evolution. In case of evolved donors (beyond Hertzsprung gap) we use the energy balance approach of Webbink (1984) with updates on estimates of CE binding energy to test whether a given system survives CE or not. It was argued that the outcome of CE is not clear in case of Hertzsprung gap donors (Belczynski et al. 2007; Pavlovskii et al. 2017). For all models we either allow for CE survival (based on energy balance) through CE with Hertzsprung gap donor (submodels A), or we eliminate such systems from our sample (submodels B).

For all models/submodels we have formed NS-NS binaries. We can calculate now the delay time from star formation to NS-NS merger for each system as:

$$t_{\rm delay} = t_{\rm evol} + t_{\rm mer,i} \tag{2}$$

where  $t_{\rm evol}$  is the time from star formation (Zero Age Main Sequence for both stars in a given binary) to the formation of the NS-NS system, and  $t_{\rm mer,i}$  is the (intrinsic) merger time: time from NS-NS formation to final coalescence of two NSs. The evolutionary time is set by the evolution of massive stars that form

NSs (usually several to several tens of Myr), while the intrinsic merger time is set by the two NS masses and orbital separation and eccentricity (Peters (1964); it can range from 0 to very large values for wide orbits). In Figures 1, 2, 3, 4, 5, and 6 we show delay time distributions for some of our evolutionary models.

# 3. Criteria for a NS-NS binary selection from models

# 3.1. Milky Way NS-NS merger rates

In each simulation, we evolve  $N_{\rm mbin}=2\times10^6$  massive binaries: primary in mass range 5–150  ${\rm M}_{\odot}$  and secondary in mass range 3–150  ${\rm M}_{\odot}$ . With our adopted binary fraction of 50%, and our adopted broken power-law initial mass function (IMF) with slope of –2.3 for massive stars our total simulated mass (extended to hydrogen burning limit: 0.08  ${\rm M}_{\odot}$ ) is  $M_{\rm sim}=2.8\times10^8~{\rm M}_{\odot}$ . In each simulation we generate some number of NS-NS binaries with delay time shorter than age of Galactic disk (10 Gyr):  $N_{\rm nsns}$ . Assuming mass of the Galactic disk to be  $M_{\rm MW, disk}=5.17\times10^{10}~{\rm M}_{\odot}$ , and continuous star formation in Galactic disk during 10,000 Myr we can estimate Galactic disk merger rate from

$$\mathcal{R}_{\text{MW}} = \frac{M_{\text{MW,disk}}}{M_{\text{sim}}} \frac{N_{\text{nsns}}}{10,000} Myr^{-1}.$$
 (3)

Milky Way disk merger rates for various models are reported in Tables 2 and 3.

## 3.2. Current Milky Way NS-NS merger times

We assign synthetic binaries that form NS-NS systems Galactic birth time:  $t_{birth}$  in range 0–10 Gyr; these times are drawn from uniform distribution that may well represent a continuous star formation rate and age of the Galactic disk. Synthetic binaries form NS-NS systems at time:  $t_{\text{form}} = t_{\text{birth}} + t_{\text{evol}}$ . From the NS-NS formation time to current Galactic disk age (10Gyr) we evolve NS-NS systems according to loss of angular momentum through emission of gravitational waves. This leads to a decrease of the orbital parameters a and e. We record current Galactic time NS-NS orbital properties:  $a_{MW}$  and  $e_{MW}$  (note that these values may differ quite significantly from the binary orbital parameters at the formation of NS-NS system). Note also that some NS-NS may have merged before reaching the current Galactic time, and that some binaries may not have formed a NS-NS by the current Galactic time (these systems are not included in the follow-up analysis):

- 1. the synthetic NS-NS binaries at Galactic current time  $t_{\rm galax} = 10$  Gyr are selected
- 2. the NS-NS current merger time is calculated:  $t_{\rm mer,MW}$  based on the current Galactic orbital parameters  $a_{\rm MW}$  and  $e_{\rm MW}$
- 3. if  $t_{\text{mer,MW}} > t_{\text{cutoff}} = 6 \times 10^5 \text{ Gyr NS-NS}$  is removed: merger time longer than for the longest observed NS-NS system
- 4. a radio (young) pulsar is defined as a NS with age:  $t_{\rm age} < \tau_{\rm radio}$  yr, where  $\tau_{\rm radio}$  is radio pulsar lifetime drawn from specific distribution (see Fig. B.1)
- 5. a recycled pulsar is defined as a NS with age:  $t_{\rm age} < t_{\rm recyc}$  yr and entire (RLOF+CE+WIND) accreted mass:  $dM > dM_{\rm rec} = 0.1~{\rm M}_{\odot}$ .  $t_{\rm recyc}$  is recycled pulsar lifetime drawn from specific distribution (see Fig. B.2)
- NS-NS systems without at least one radio or one recycled pulsar at current Galactic time are removed (as non-detectable in radio)

the leftover NS-NS binaries are the current Galactic radiodetectable population.

The properties of such selected sample of model NS-NS systems are compared with the current merger times of the known Galactic field NS-NS binaries: see Table 2 and Figures 7, 8, 9, and 10.

# 3.3. NS-NS merger rate in elliptical galaxies

We use the Illustris cosmological simulation (Vogelsberger et al. 2014; Snyder et al. 2015) to estimate the mass of all elliptical galaxies within cube with side of L = 100 Mpc. The volume of such cube (0.001 Gpc<sup>3</sup>) approximately corresponds to volume in which LIGO/Virgo was able to detect NS-NS mergers in O1/O2 runs. Following details discussed in Appendix A of Belczynski et al. (2018) this mass is  $M_{\rm ell,tot} = 1.1 \times 10^{14} \, \rm M_{\odot}$ . Since our simulation mass is only  $M_{\rm sim} = 2.8 \times 10^8 \, \rm M_{\odot}$  we will have to multiply number of NS-NS binaries that we form in each model by  $F_x = M_{\rm ell,tot}/M_{\rm sim} = 3.9 \times 10^5$ . This gives us total number of NS-NS binaries formed in all ellipticals within LIGO/Virgo reach. This number then needs to be modified by adopted star formation history in elliptical galaxies. We perform two calculations. In one we assume that all ellipticals in local Universe are 10 Gyr old (e.g., approximately NGC4993), and in the other that ages of ellipticals in local Universe are uniformly distributed in range 1-11 Gyr (Gallazzi et al. 2006). We assume that star formation in ellipticals was a burst event: all stars formed at the same time corresponding to the age of a given elliptical galaxy. Final current time (present) local rate of NS-NS mergers ( $\mathcal{R}_{ell}$ ) from elliptical galaxies is estimated with the use of NS-NS delay time distribution found in our models (see Sec. 4.1). The rates for all the models are listed in Table 3.

## 4. Results

## 4.1. Galactic NS-NS delay time distribution

Note that delay times (from ZAMS to merger; eq. 2) for NS-NS binaries are not known as exact recycled (majority of Galactic population) pulsar ages cannot be established. However, the delay time distribution is a primary factor (along star forming mass) setting the NS-NS merger rate in any host galaxy.

Figures 1, 2, and 3 show delay time distributions for NS-NS binaries in models M10, NN3, NN8. These are typical models, that adopt high to moderate natal kicks for CC NSs and zero natal kicks for ECS NSs, non-conservative RLOF with 50–80% of mass loss from binary, and fully efficient CE evolution ( $\alpha_{\rm CE}=1$ ). The distributions for all these models (and submodels A and B) are very similar and they follow a power-law  $t_{\rm delay}^{-1}$  over many orders of magnitude. Distributions begin at  $\sim 10-100$  Myr and end around  $10^{21}$  Gyr. Note the gap in the delay time distribution at times  $10^7-10^{15}$  Gyr. This gap separates the systems that formed through CE phase (left of the gap; short delays) and that did not evolve through CE phase (right of the gap; long delays).

It is clear that the merger rate of NS-NS systems decreases steeply from the end of star formation in a given host galaxy. For example, a galaxy with a burst of star formation within last 100 Myr would have a NS-NS merger rate 100 times larger than an elliptical galaxy of the same mass that had its burst of star formation 10 Gyr ago. A spiral host galaxy that forms stars in continuous fashion would generate a merger rate between these two extreme cases. This has two consequences.

- 1. NGC4993, in which GW170817 was found, had a peak of star formation ~ 11 Gyr ago (Blanchard et al. 2017) and therefore is a very unlikely galaxy to host the first NS-NS merger. The majority of NS-NS mergers are predicted to happen quickly after star formation; in starburst or spiral galaxies, with only a small fraction occurring in old ellipticals.
- 2. The evolutionary NS-NS merger rate predictions that are pushed to reach 300 500 Gpc<sup>-3</sup> yr<sup>-1</sup> (Chruslinska et al. 2018; Kruckow et al. 2018; Vigna-Gómez et al. 2018; Mapelli & Giacobbo 2018) are indeed consistent with the LIGO/Virgo rate estimate (110–3840 Gpc<sup>-3</sup> yr<sup>-1</sup>). However, these predictions are based on overall star formation in the local Universe in *all* sorts of host galaxies. These predictions produce steep power-law delay times for NS-NS binaries as in our models described above (M10, NN3 or NN8). If the rates are recalculated *only* for old host galaxies (resembling NGC4993), they drop by ~ 2 orders of magnitude and are thus in tension with the LIGO/Virgo estimate (Belczynski et al. 2018).

The power-law shape of the delay time distribution of NS-NS binaries is a generic outcome of modern population synthesis predictions and is naturally explained by the underlying physics. The initial orbital separation distribution for massive O/B stars follows approximately a power-law  $\alpha$   $a^{-1}$ . Evolutionary processes in close binary systems (in particular CE phase) reduce initial binary separations by 1-2 orders of magnitude, producing an even steeper power-law distribution of separations at NS-NS formation  $\alpha$   $\alpha$  After NS-NS formation, binary orbit decays due to emission of gravitational radiation (GR) at the rate that is firmly established and strongly depends on orbital separation of two NSs:  $t \alpha$   $\alpha$  (Peters 1964). Assuming that the distribution of orbital separations at the time of formation of the NS-NS binary can be described by a power-law  $dN/da \alpha \alpha^{-\beta}$ , we obtain the distribution of the merger times  $dN/dt_{merg} \alpha t^{-\beta/4-3/4}$ . The exponent only weakly depends on  $\beta$  and for  $\beta = 1$  we obtain  $dN/dt_{merg} \alpha t^{-1}$ , while for  $\beta = 3$  we obtain  $dN/dt_{merg} \alpha t^{-1.5}$ 

Figures 4, 5, 6 show delay time distributions for NS-NS binaries in models NN13, NN1, NN6. These models include very low natal kicks as imposed by Bray & Eldridge (2018) formula (NN1, NN6) or zero natal kicks (NN13) for all CC and ECS NSs. Additionally, very high CE efficiency is assumed ( $\alpha_{CE} = 10$ ) in models NN13 and and NN6. These are rather extreme assumptions, as some NSs in NS-NS binaries are believed to receive at least small to moderate natal kicks, and it is rather unlikely that there is as much extra energy in binary as 10 times orbital energy available for CE ejection. Ignoring this for the moment we examine corresponding delay time distributions. Although these distributions also follow power-law trend  $(t_{delay}^{-1})$  there are some differences from other models. Notably the distributions show some bumps, some of which peak around 10 Gyr, and distributions for submodels B start at rather late times (~ 1 Gyr) reaching peak at 10 Gyr. This can possibly help to deliver high NS-NS merger rates at late times after star formation. In fact, for model NN13.A and NN6.A the current NS-NS merger rate from elliptical galaxies within LIGO/Virgo reach is  $\sim 156-561 \, \mathrm{Gpc}^{-3} \, \mathrm{yr}^{-1}$ and thus consistent with LIGO/Virgo estimate. Even model NN1.B rate from elliptical galaxies (50.6 Gpc<sup>-3</sup> yr<sup>-1</sup>) is only factor of 2 below LIGO/Virgo 90% confidence level lower limit. Obviously small NS natal kicks do not disrupt progenitor binaries increasing merger rates, while high CE efficiency allows for the increased formation of close NS-NS binaries with long delay times.

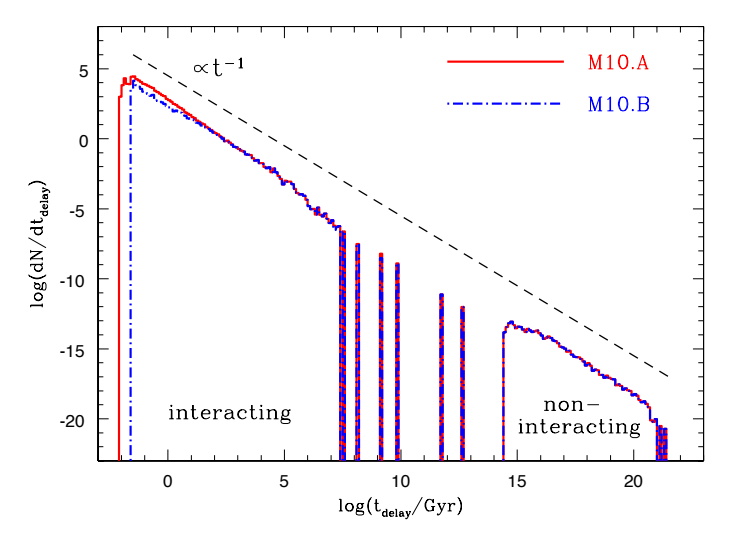
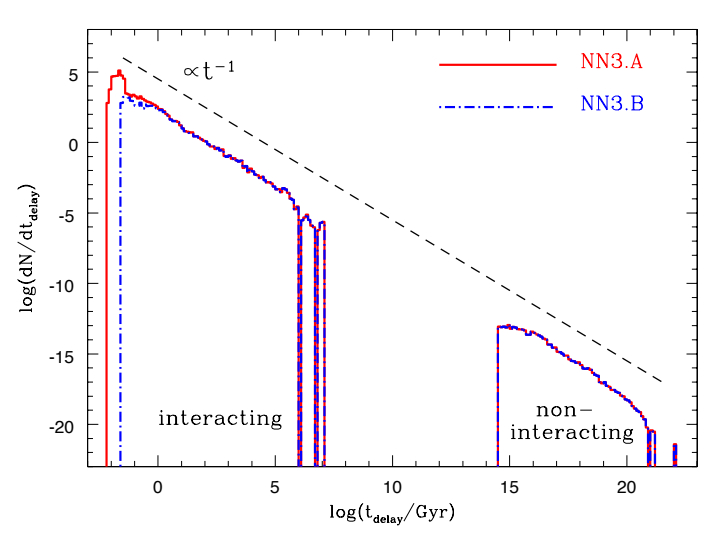
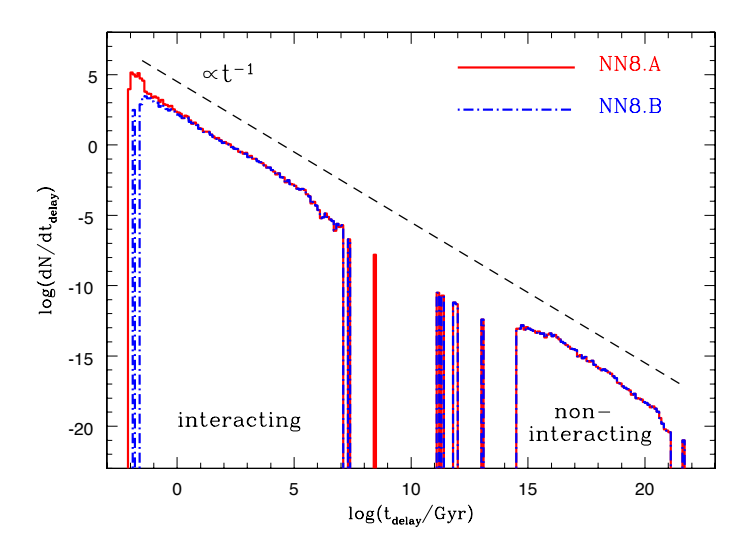


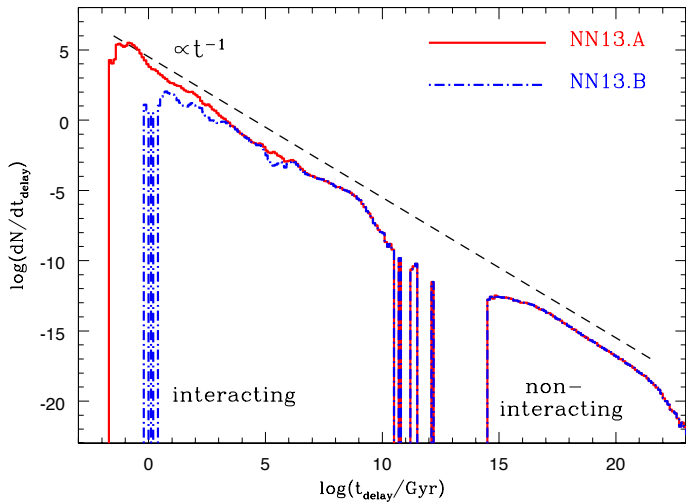
**Fig. 1.** Model M10: NS-NS delay time distribution. Note generic power-law ( $\propto t^{-1}$ ) shape of the distribution. We indicate NS-NS populations that formed out of interacting (common envelope) and non-interacting (no common envelope) binary progenitor systems.



 $\begin{tabular}{ll} \textbf{Fig. 2.} & Model NN3: NS-NS delay time distribution. Labels same as in Figure 1. \end{tabular}$ 



 $\begin{tabular}{ll} Fig. 3. & Model NN8: NS-NS delay time distribution. Labels same as in Figure 1. \end{tabular}$ 



 $\begin{tabular}{ll} \textbf{Fig. 4.} & Model NN13: NS-NS delay time distribution. Labels same as in Figure 1. \end{tabular}$ 

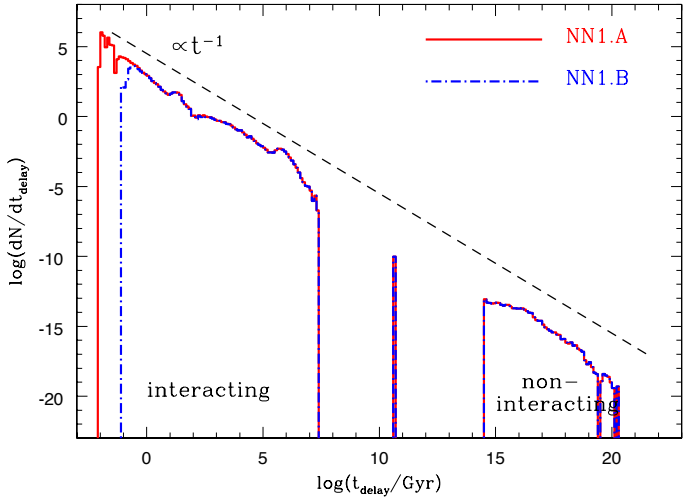
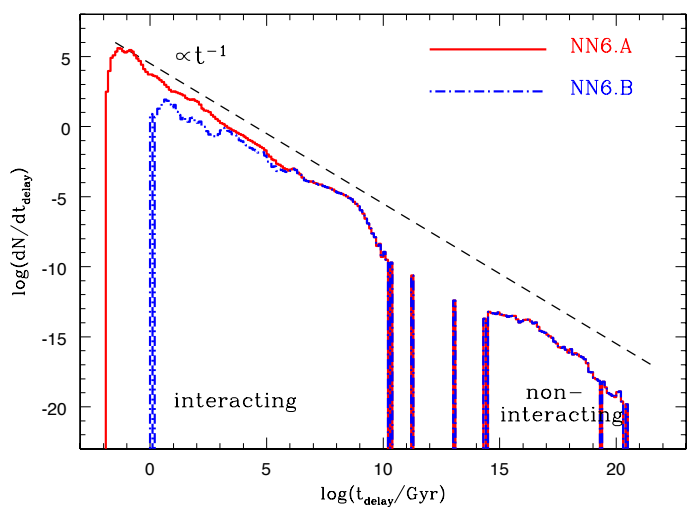


Fig. 5. Model NN1: NS-NS delay time distribution. Labels same as in Figure 1.



 $\begin{tabular}{ll} \textbf{Fig. 6.} & Model NN6: NS-NS delay time distribution. Labels same as in Figure 1. \end{tabular}$ 

## 4.2. Current NS-NS Galactic merger time distribution

Note that the current NS-NS Galactic merger time distribution (observable) is different from merger time distribution at NS-NS formation (intrinsic). We transform our model NS-NS delay time distributions through continuous Galactic disk star formation applying radio-detectability criteria to obtain the current NS-NS Galactic merger time distributions (see Sec. 3.2).

Figures 7 and 8 show the cumulative distribution of current Galactic NS-NS merger times for models M10, NN2, NN3, and NN4 for both submodels A and B. For comparison we also show the observed cumulative distribution of the 16 Galactic field NS-NS binaries (see Tab. 1). These models encompass rather broad assumptions on natal kicks; from all NSs receiving high natal kicks (NN2;  $\sigma=265~{\rm km~s^{-1}}$  with no decrease due to fallback), through high CC NS natal kicks and no ECS NS natal kicks (NN3), to no natal kicks at all (NN4). These models also probe the conservativeness of RLOF from 80% mass loss (NN2, NN3, NN4) to 50% (M10). We note that these model distributions are very similar to the observed distribution. In particular, all these model distributions have a significant probability ( $\sim 15\%-87\%$ ) of being drawn from the same underlying distribution as the observed sample: see KS test p-values given in Table 2.

In Table 2 we also list the fraction of short merger time NS-NS systems versus long merger time systems. We choose 30 Gyr as a dividing line between short and long merger time systems. This time corresponds to the mid-point between short and long merger times systems known in the Galaxy. We find that many models are close to the 50%–50% observed ratio of short–long merger time systems (see Tab. 1). Specifically, the models discussed above (M10, NN2, NN3, NN4) show fraction of long merger time systems in the range: 27–58%.

Figures 9, and 10 show the cumulative distribution of current Galactic NS-NS merger times for models NN1, NN5,NN6, and NN13. These models encompass some of our extreme assumptions on input physics. In models NN1, NN5, NN6 we employ Bray & Eldridge (2018) natal kicks while varying CE efficiency:  $\alpha_{\rm CE}=0.1,1.0,10$ , respectively. In model NN13 NSs do not receive any natal kicks and very high CE efficiency is used  $\alpha_{\rm CE}=10$ . We note that these models do not match observations as well as the other models (M10, NN2, NN3, and NN4 shown in Fig. 7 and 8). In particular, the probability that these models are drawn from the same distribution as the observed sample can be very small and is found in the range  $\sim 0.01-37\%$  for all these four models. The fraction of the long current merger time systems varies in wide range for these models 20-90% for these models (see Tab. 1).

## 4.3. Milky Way NS-NS merger rate vs LIGO/Virgo rate

In Table 3 we report the Galactic merger rate of NS-NS systems (see Sec. 3.1) along with the corresponding rate density on NS-NS mergers from elliptical galaxies in local Universe (see Sec. 3.3) for all our models. The range reported in Galactic model NS-NS merger rates corresponds to an assumption on the star forming mass in the Galactic disk. The low rates correspond to the disk mass of  $3.5 \times 10^{10}~M_{\odot}$  that was used in our previous estimates (Belczynski et al. 2010b; Dominik et al. 2012) while the high rates correspond to the disk mass of  $5.17 \times 10^{10}~M_{\odot}$  recently estimated by Licquia & Newman (2015). The range reported in model NS-NS merger rate density in elliptical galaxies corresponds to assumed age of ellipticals (their stellar populations): all ellipticals 10 Gyr old (left hand side values) or age distributed uniformly in range 1–11 Gyr (right hand side values).

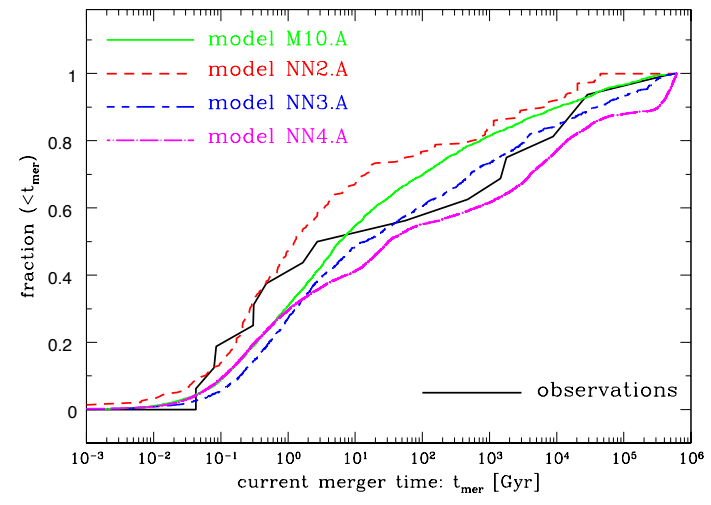


**Fig. 7.** The cumulative distribution of the observed current merger times of NS-NS systems in the Milky Way and the ones predicted by models M10.A, NN2.A, NN3.A and NN4.A with the inclusion of selection effects described in Section 3.

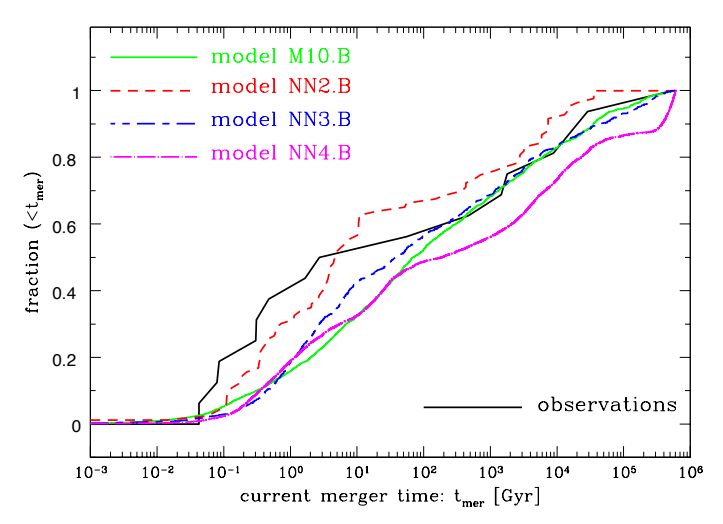
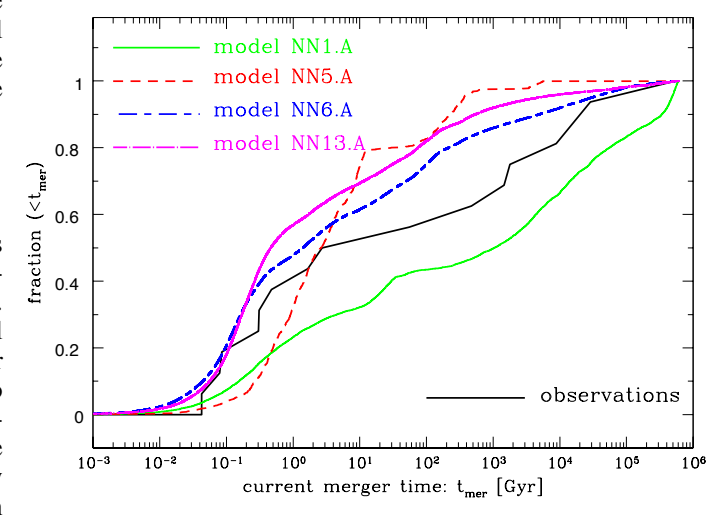
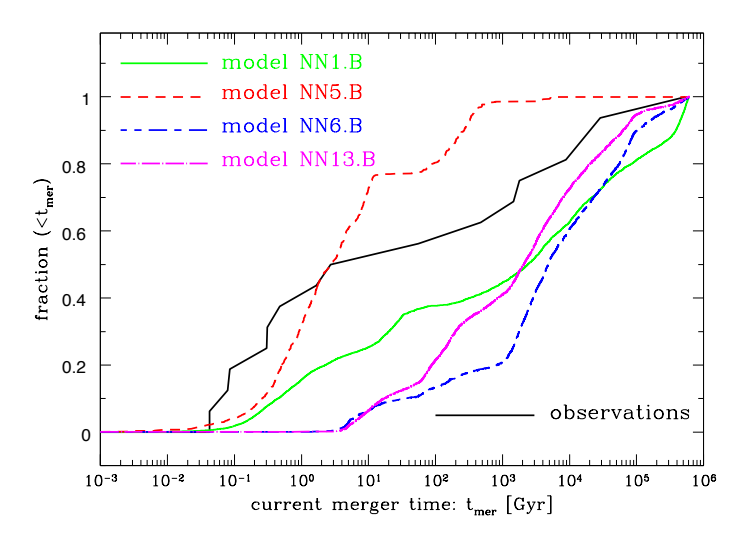


Fig. 8. Same as Figure 7 but for models M10.B, NN2.B, NN3.B and NN4.B.



**Fig. 9.** Same as Figure 7 but for models NN1.A, NN5.A, NN6.A and NN13.A.



**Fig. 10.** Same as Figure 7 but for models NN1.B, NN5.B, NN6.B and NN13.B.

For comparison with models we also list empirical estimates in Table 3. The empirical Galactic merger rate estimates are based on the 8 Galactic NS-NS systems with merger times shorter than the Hubble time:  $28-72~{\rm Myr}^{-1}$  (Pol et al. 2018) and  $6.6-190~{\rm Myr}^{-1}$  (see App. A). For empirical NS-NS merger rate density in elliptical galaxies in local Universe we adopt LIGO/Virgo estimate:  $110-3840~{\rm Gpc}^{-3}~{\rm yr}^{-1}$ .

Investigation of Table 3 allows us to note:

- 1. Some models may be rejected based on comparison with Galactic NS-NS merger rates: NN2.B (high Hobbs et al. (2005) natal kicks for all NSs with HG CE not allowed), NN14.B (high Hobbs et al. (2005) natal kicks with fallback for all NSs with HG CE not allowed), NN7.B (medium Hobbs et al. (2005) natal kicks for all NSs with HG CE not allowed), NN4.A (no natal kicks for all NSs with HG CE allowed), NN13.A (no natal kicks for all NSs and very high CE efficiency with HG CE allowed), NN1.A (Bray & Eldridge (2018) natal kicks with HG CE allowed), and NN6.A/B (Bray & Eldridge (2018) natal kicks with very high CE efficiency independent of treatment of CE survival with HG donor).
- 2. Two models generate NS-NS merger rate densities in local Universe elliptical galaxies high enough to overlap with LIGO/Virgo estimate: NN13.A (zero natal kicks for all NSs with HG CE allowed) and NN6.A (Bray & Eldridge (2018) natal kicks with very high CE efficiency and HG CE allowed). However, these models produce extremely high Galactic NS-NS merger rates ( $\gtrsim 1000~{\rm Myr}^{-1}$ ) that significantly exceed empirical Milky Way rate estimates ( $\lesssim 200~{\rm Myr}^{-1}$ ).
- 3. Majority of models generate NS-NS merger rates that are consistent with the Milky Way empirical merger rate estimates: NN2.A, NN14.A, NN7.A, NN3.A/B, NN8.A/B, M10.A/B, NN11.A/B, NN9.A/B, NN10.A/B, NN12.A/B, NN4.B, NN13.B, NN5.A/B, and NN1.B. None of these models deliver rate of NS-NS mergers in elliptical galaxies consistent with LIGO/Virgo estimate. Note that for comparisons we use larger Galactic NS-NS merger model rates as they correspond to updated mass of the Galactic disk.

#### 5. Conclusions

We have analyzed the validity of evolutionary predictions in the context of the recent gravitational-wave detection of the first NS-NS merger and taking into account the already rich population of 16 Galactic field NS-NS binaries. Generally, evolutionary predictions are consistent with the Galactic population of NS-NS binaries recovering the Galactic merger rates and observed merger time distribution. However, at the same time, the models that are in agreement with the Galactic observations, generate local cosmic NS-NS merger rates in elliptical galaxies that are not consistent with LIGO/Virgo estimate.

Evolutionary models predict that currently (low redshifts) the majority of NS-NS mergers should be found in systems with ongoing or recent star formation, due to a steep-power law  $(\propto t^{-1})$  delay time distribution (see also O'Shaughnessy et al. 2010). Note that Advanced LIGO/Virgo even at its design sensitivity will be only able to discover NS-NS mergers at lowredshifts ( $z \leq 0.1$ ). For higher redshifts, models predict the increasing contribution of elliptical hosts, as the time between star formation in elliptical galaxies (~ 1-10 Gyr ago) and a given redshift decreases. Our models appear to be broadly consistent with observations of short GRBs (O'Shaughnessy et al. 2008a). Fong et al. (2013) estimated the frequency of short GRBs among late type hosts (60-80%) and early type hosts galaxies (20-40%). This analysis includes also host-less and inconclusive short GRB cases. If only confirmed-host short GRBs are used, the fraction of short GRBs in early type hosts (e.g., ellipticals) drops down to  $\sim 20\%$ .

There is a set of population synthesis calculations performed with the BPASS code (Eldridge et al. 2017) that generates large Galactic NS-NS merger rates: a most likely value of 386 Myr with uncertainty range of 149–543 Myr<sup>-1</sup> (Bray & Eldridge 2018; Eldridge et al. 2018). This estimate was obtained for solar metallicity (Z = 0.02) and a Galactic disk mass of  $3.5 \times 10^{10}$  M<sub> $\odot$ </sub>. If we correct this rate for more realistic Galactic disk mass:  $5.17 \times 10^{10} \ M_{\odot}$  (Licquia & Newman 2015), then the BPASS NS-NS merger rate is 571 Myr<sup>-1</sup> with an uncertainty range: 221– 804 Myr<sup>-1</sup>. This high rate seem to be at odds with the empirical Galactic merger rates: 28–72 Myr<sup>-1</sup> (Pol et al. 2018) and 6.6– 190 Myr<sup>-1</sup> (see App. A). This high rate is obtained with a new prescription of NS natal kicks that is based on the ratio of supernova ejecta mass to NS mass predicted in models. We have tested this new prescription in our calculations. And in fact this prescription results in almost no NS natal kicks increasing significantly NS-NS merger rate.

We find that it is possible to construct evolutionary models that generate NS-NS merger rates in elliptical galaxies that are consistent with the LIGO/Virgo estimate. These models employ no or very low natal NS kicks (e.g., Bray & Eldridge (2018) natal kicks) and very high CE efficiency. However, these models are not consistent with the Galactic population of NS-NS binaries. For example, Galactic merger rates generated in these models are much higher ( $\sim 1000~{\rm Myr}^{-1})$  than estimated from observations ( $< 200~{\rm Myr}^{-1})$ .

Thus we are left with the tension between evolutionary models supported by the Galactic NS-NS observations and the LIGO/Virgo early detection of a NS-NS merger in an old host galaxy. Potential solutions of this problem may include:

 The LIGO/Virgo detection was a statistical fluctuation, and the following detections will be associated with regions with ongoing or recent star formation. After all, models do predict NS-NS mergers in old hosts, alas at low rates. If this is

- the case, this will be quickly resolved by near-future observations by LIGO/Virgo at increased sensitivity during the O3 run in 2019.
- 2. If the above is not true then it it possible that the solution sits in a part of multi-dimensional parameter space that we did not probe with our very limited models. Massive multi-dimensional parameter studies (e.g., O'Shaughnessy et al. 2008b) are needed to confirm or reject such hypothesis. Here we have only attempted to probe a small part of parameter space to serve as an initial step for such future studies.
- 3. If the above is not true then if LIGO/Virgo keep detecting NS-NS mergers in old hosts (as it may be indicated by GRB 150101B; see Sec. 1) then this will call for a revision of models of isolated binary evolution. Such a revision would need to preserve typically short delay times produced by current models for star forming galaxies (e.g., the Milky Way), but it will need to generate typically long delay times for old galaxies (e.g., ellipticals).
- 4. If the above is not true then isolated binary evolution model that connect NS-NS formation directly to star forming mass is not the correct solution in the case of GW170817. It was already proposed that dynamical interactions between stars (or compact objects) in two merging galaxies may induce enhanced NS-NS formation (Palmese et al. 2017). In this context, even with no significant star formation in a conceivable recent minor merger in NGC 4993, it may have been possible that a NS-NS merger formed through enhanced dynamical interactions.

Acknowledgements. KB acknowledges support from the Polish National Science Center (NCN) grants OPUS (2015/19/B/ST9/01099), Maestro (2015/18/A/ST9/00746) and LOFT/eXTP (2013/10/M/ST9/00729). We would like to thank thousands of Universe@home users that have provided their personal computers and phones for our simulations, and in particular to K. Piszczek (program IT manager). TB acknowledges support from the grant FNP grant TEAM-2016-3/19.

Table 2. Properties of NS-NS binaries<sup>a</sup>

Name	short <sup>b</sup>	long	p-value <sup>c</sup>	$\mathcal{R}_{MW}$ [Myr <sup>-1</sup> ]
observations	50%	50%		$28-72^d$
				6.6–190 <sup>e</sup>
NN2.A	73%	27%	0.260	13.5–20.0
NN2.B	64%	36%	0.813	0.9–1.3
NINTI 4 A	0.201	100	0.021	22 6 22 4
NN14.A NN14.B	82% 77%	18% 23%	0.021 0.067	22.6–33.4
ININ14.D	11%	25%	0.007	1.5–2.2
NN7.A	62%	38%	0.445	32.4-48.0
NN7.B	53%	47%	0.532	3.1–4.6
111112	22,0	.,,,,	0.002	0.1
NN3.A	54%	46%	0.587	38.4-56.8
NN3.B	48%	52%	0.165	10.8-16.0
NN8.A	43%	57%	0.329	45.0–66.6
NN8.B	34%	66%	0.091	10.6–15.7
N/10 A	6201	2701	0.267	52 6 70 2
M10.A	63%	37% 58%	0.367	53.6–79.3
M10.B	42%	38%	0.145	17.4–25.8
NN11.A	57%	43%	0.731	61.1–90.4
NN11.B	52%	48%	0.376	7.8–11.5
111111.2	3270	10 /0	0.570	7.0 11.0
NN9.A	51%	49%	0.875	67.6-100
NN9.B	46%	54%	0.318	11.0-16.3
NN10.A	36%	64%	0.246	76.9–114
NN10.B	29%	71%	0.058	16.0–23.7
NINI1O A	5001	500	0.067	106 106
NN12.A	50%	50%	0.967	126–186
NN12.B	43%	57%	0.283	21.8–32.3
NN4.A	49%	51%	0.873	251–371
NN4.B	43%	57%	0.238	48.9–72.4
1111112	1370	5776	0.250	10.5 72.1
NN13.A	75%	25%	0.044	1208-1788
NN13.B	13%	87%	$\sim 10^{-4}$	6.7-9.9
NN5.A	80%	20%	0.008	11.9–17.6
NN5.B	77%	23%	0.007	11.5–17.0
			0.4.0	.=0=
NN1.A	40%	60%	0.368	179–265
NN1.B	34%	66%	0.108	37.0–54.8
NN6.A	67%	33%	0.156	961–1422
NN6.A NN6.B	10%	33% 90%	$\sim 10^{-4}$	961–1422 4.1–6.1
ININU.D	10%	90%	~ 10	4.1-0.1

## Notes.

<sup>&</sup>lt;sup>a</sup> Comparison of observed and model current merger time distributions.

<sup>&</sup>lt;sup>b</sup> short:  $t_{\text{mer}} < 30 \text{ Gyr}$ , long:  $t_{\text{mer}} > 30 \text{ Gyr}$ .

<sup>&</sup>lt;sup>c</sup> Probability that observations and model were drawn from the same delay time distribution (KS test).

 $<sup>^</sup>d$  Estimate from Pol et al. (2018) with peak probability value of  $\mathcal{R}_{\rm MW}$  =42 Myr  $^{-1}$  .

<sup>&</sup>lt;sup>e</sup> Estimate presented in App. A.

Table 3. NS-NS merger rates: sorted by natal kick and increasing Galactic rates

Name	CC kick <sup>a</sup>	ECS kick <sup>b</sup>	$\alpha_{\mathrm{CE}}^{c}$	(acc/eje) <sub>RLOF</sub> <sup>d</sup>	$\mathcal{R}_{\mathrm{MW}}$ [Myr <sup>-1</sup> ] <sup>e</sup>	$\mathcal{R}_{\mathrm{ell}}$ [ $\mathrm{Gpc^{-3}\ yr^{-1}}$ ] $^f$
observations					$\begin{array}{c} 28-72^g \\ 6.6-190^h \end{array}$	110–3840 <sup>i</sup>
NN2.A	Hobbs: 265 km s <sup>-1</sup>	OFF: –	1.0	0.2/0.8	13.5–20.0	0.8–2.3
NN2.B	Hobbs: 265 km s <sup>-1</sup>	OFF: –	1.0	0.2/0.8	0.9–1.3	0.8–2.3
11112.15		011.	1.0	0.2/0.0	0.5 1.5	0.0 2.3
NN14.A	HobbsFB: 265 km s <sup>-1</sup>	OFF: –	1.0	0.2/0.8	22.6–33.4	0.8–3.0
NN14.B	HobbsFB: 265 km s <sup>-1</sup>	OFF: –	1.0	0.2/0.8	1.5–2.2	0.8–2.0
NN7.A	Hobbs: 133 km s <sup>-1</sup>	ON: 66 km s <sup>-1</sup>	1.0	0.2/0.8	32.4–48.0	1.2–6.2
NN7.B	Hobbs: 133 km s <sup>-1</sup>	ON: 66 km s <sup>-1</sup>	1.0	0.2/0.8	3.1–4.6	1.2–4.1
NN3.A	HobbsFB: 265 km s <sup>-1</sup>	ON: 0 km s <sup>-1</sup>	1.0	0.2/0.8	38.4–56.8	6.3–21.0
NN3.B	HobbsFB: 265 km s <sup>-1</sup>	ON: $0 \text{ km s}^{-1}$	1.0	0.2/0.8	10.8–16.0	5.9–18.9
NN8.A	Hobbs: 133 km s <sup>-1</sup>	ON: 0 km s <sup>-1</sup>	1.0	0.2/0.8	45.0–66.6	8.3–19.6
NN8.B	Hobbs: 133 km s <sup>-1</sup>	ON: 0 km s <sup>-1</sup>	1.0	0.2/0.8	10.6–15.7	7.5–15.6
M10.A	HobbsFB: 265 km s <sup>-1</sup>	ON: 0 km s <sup>-1</sup>	1.0	0.5/0.5	53.6–79.3	11.4–51.4
M10.A M10.B	HobbsFB: 265 km s <sup>-1</sup>	ON: $0 \text{ km s}^{-1}$	1.0	0.5/0.5	17.4–25.8	18.5–22.1
NN11.A	Hobbs: 66 km s <sup>-1</sup>	OFF: –	1.0	0.2/0.8	61.1–90.4	4.7–13.1
NN11.B	Hobbs: 66 km s <sup>-1</sup>	OFF: –	1.0	0.2/0.8	7.8–11.5	4.3–11.8
NN9.A	Hobbs: 66 km s <sup>-1</sup>	ON: 33 km s <sup>-1</sup>	1.0	0.2/0.8	67.6–100	3.9–18.4
NN9.B	Hobbs: 66 km s <sup>-1</sup>	ON: $33 \text{ km s}^{-1}$	1.0	0.2/0.8	11.0–16.3	3.9–16.3
NN10.A	Hobbs: 66 km s <sup>-1</sup>	ON: 0 km s <sup>-1</sup>	1.0	0.2/0.8	76.9–114	7.9–29.9
NN10.B	Hobbs: 66 km s <sup>-1</sup>	ON: 0 km s <sup>-1</sup>	1.0	0.2/0.8	16.0–23.7	7.5–27.7
NN12.A	Hobbs: 33 km s <sup>-1</sup>	OFF: –	1.0	0.2/0.8	126–186	13.4–33.1
NN12.B	Hobbs: 33 km s <sup>-1</sup>	OFF: –	1.0	0.2/0.8	21.8–32.3	13.4–31.5
NN4.A	Hobbs: 0 km s <sup>-1</sup>	OFF: –	1.0	0.2/0.8	251–371	23.2–72.1
NN4.B	Hobbs: 0 km s <sup>-1</sup>	OFF: –	1.0	0.2/0.8	48.9–72.4	23.2–70.8
NN13.A	Hobbs: 0 km s <sup>-1</sup>	OFF: –	10	0.2/0.8	1208–1788	186–561
NN13.B	Hobbs: 0 km s <sup>-1</sup>	OFF: –	10	0.2/0.8	6.7–9.9	29.9–25.2
NN5.A	BE18: 100/ – 170 km s <sup>-1</sup>	OFF: –	0.1	0.2/0.8	11.9–17.6	11.8–22.9
NN5.B	BE18: 100/ – 170 km s <sup>-1</sup>	OFF: –		0.2/0.8	11.5–17.0	11.8–22.9
NN1.A	BE18: 100/ – 170 km s <sup>-1</sup>	OFF: –	1.0	0.2/0.8	179–265	15.3–51.2
NN1.B	BE18: 100/ – 170 km s <sup>-1</sup>	OFF: –	1.0	0.2/0.8	37.0–54.8	15.3–50.6
NN6.A	BE18: 100/ – 170 km s <sup>-1</sup> BE18: 100/ – 170 km s <sup>-1</sup>	OFF: –	10	0.2/0.8	961–1422	156–471
NN6.B		OFF: –	10	0.2/0.8	4.1–6.1	12.6–15.1

## Notes

Article number, page 10 of 12

<sup>&</sup>lt;sup>a</sup> Core collapse SN NS natal kicks. Hobbs: Maxwellian distribution with a given 1-D  $\sigma$ ; HobbsFB: Maxwellian distribution with a given 1-D  $\sigma$  lowered by fall-back; BE18: Bray & Eldridge kicks with a given  $\alpha$  and  $\beta$ .

 $<sup>^</sup>b$  Electron capture SN NS natal kicks. OFF: all NSs form through CC SNe; ON: ECS allowed with a kick from Maxwellian distribution with a given 1-D  $\sigma$  with fall back as for CC kicks.

<sup>&</sup>lt;sup>c</sup> Common envelope efficiency

<sup>&</sup>lt;sup>d</sup> Mass fraction of donor mass transfer accreted by donor/ejected from binary during stable RLOF

 $<sup>^</sup>e$  The Milky Way NS-NS merger rate. Left–right hand side values correspond to Galactic disk mass of  $3.5 \times 10^{10}~M_{\odot}$ – $5.17 \times 10^{10}~M_{\odot}$ .

f Local cosmic (z = 0) merger rate density for NS-NS systems formed only in elliptical galaxies. Left–right hand side values correspond to assumed age of ellipticals (their stellar populations): all ellipticals 10 Gyr old – age distributed uniformly in range 1–11 Gyr.

<sup>&</sup>lt;sup>8</sup> 90% confidence level, with peak value of 42 Myr<sup>-1</sup> from Pol et al. (2018).

<sup>&</sup>lt;sup>h</sup> Conservative rate range described in App. A.

<sup>&</sup>lt;sup>i</sup> LIGO/Virgo 90% confidence level, with peak value of ~ 1000 Gpc<sup>-3</sup> yr<sup>-1</sup>

# Appendix A: NS-NS rate estimate

We estimate the galactic NS-NS merger rate  $\mathcal{R}_{MW}$  from the observed number of coalescing NS-NS binaries ( $N_{psr} = 8$ ) using two simplifying and phenomenologically motivated assumptions. First, we assume that the NS-NS population can be characterized by a single population-averaged probability S to be detected in radio, expressed as  $S = \langle (f_b N_{psr})^{-1} \rangle$  where  $1/N_{psr}$ is the probability of detecting such a pulsar if it were pointing towards us, and  $1/f_b$  is the probability the pulsar beam is pointing towards us. From the observed sample and previous work, we for simplicity adopt a fiducial value of  $S = 2 \times 10^{-3}$ , though this is uncertain by as much as 50%. Second, motivated by past and present theoretical modeling, we assume that NS-NS merger time distribution  $dP/d\tau$  after a burst of star formation is proportional to  $1/\tau$ , corresponding to a cumulative fraction of mergers  $P(<\tau)$  which is roughly linear in  $\log \tau$ . Using this delay time distribution, we can estimate the fraction of binaries born at time  $t_b$  which merge on or after the present day, as  $P_{alive}(t_b) = \int_T^{\infty} (dP/d\tau)d\tau = 1 - P(< T - t_b)$ , where T is the age of the Milky Way disk. Using these two simplifying assumptions, we can show a steady-state merger rate  $\mathcal{R}_{MW}$  will lead on average to  $\mu = \mathcal{R}_{\text{MW}} \int_0^T dt_b P_{ok}(t_b) \simeq 1.26 \text{Gyr} \times \mathcal{R}_{\text{MW}} \text{ NS-NS}$  binaries overall present in the Milky Way disk at the present day, with  $\mu_{\text{tight}} = 0.081 \text{Gyr} \times \mathcal{R}_{\text{MW}}$  NS-NS binaries expected to coalesce in the near future. Accounting for selection biases, we estimate the merger rate from  $N_{psr}$  observed Galactic coalescing NS-NS binaries via  $\mathcal{R}_{MW} = N_{psr}/\mu S$ . Using the two estimates  $\mu, \mu_{\text{tight}}$  to bracket our uncertainty, we arrive at a NS-NS merger rate estimate of  $\mathcal{R}_{MW} = A(S/2 \times 10^{-3}) \text{ Myr}^{-1}$  where A is between 10–95. Allowing for uncertainty in S broadens this estimate by 50%, leading to a conservative range of NS-NS merger rate  $\mathcal{R}_{MW}$  $= 6.6-190 \,\mathrm{Myr}^{-1}.$ 

## Appendix B: Radio and recycled pulsar lifetimes

To obtain the distribution of the radio lifetimes of radio pulsars and recycled pulsars in NS-NS systems, we use PsrPopPy (Bates et al. 2014) to simulate the observed pulsar population. In these simulations, we use the Parkes Multibeam survey which was able to detect  $\sim 1100$  pulsars. We use this survey to model pulsar survey parameters (see Sec. 4.1 in Bates et al. 2014).

To simulate the radio pulsar population, we use a normal distribution for the periods of the pulsars, with mean spin period  $\langle P_s \rangle = 300$  ms and standard deviation  $\sigma_P = 100$  ms. We similarly assume a log-normal magnetic field distribution for these pulsars, with mean  $\langle \log_{10} B(G) \rangle = 12.65$  and standard deviation  $\sigma_{\log_{10}B} = 0.55$ . These pulsars are assigned a lifetime,  $\tau_{\rm r}$ , which are drawn randomly from a uniform distribution between zero and the age of the Milky Way (~10 Gyr). The period and period derivative of the pulsars are evolved using the magnetic dipole model (see Sec. 3 in Bates et al. 2014) over their lifetime. If these pulsars cross the "death-line" (Chen & Ruderman 1993) during their lifetime, they will not be observable and are removed from the simulation. Finally, we determine if the pulsars that are alive are detectable in the Parkes Multibeam survey (see Sec. 4 in Bates et al. 2014). We keep generating such pulsars in the simulation until we detect the 1059 radio pulsars detected by the Parkes Multibeam Survey (Manchester et al. 2005). The distribution of the radio lifetimes of the entire population so generated (i.e., not only the 1059 pulsars detected in the survey) is shown in Fig. B.1.

We follow the same process as above to generate a distribution of the radio lifetimes for the recycled pulsars found in

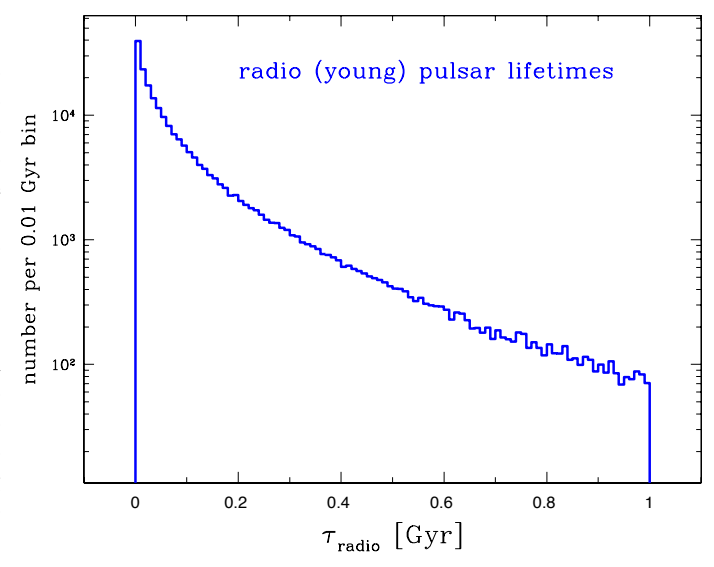


**Fig. B.1.** Radio (young) pulsar lifetime distribution. Note that majority (90%) of radio pulsars have short lifetimes ( $t_{\text{radio}} < 315 \text{ Myr}$ ). The average lifetime is  $t_{\text{radio,ave}} = 116 \text{ Myr}$ , while median is  $t_{\text{radio,med}} = 52.2 \text{ Myr}$ .

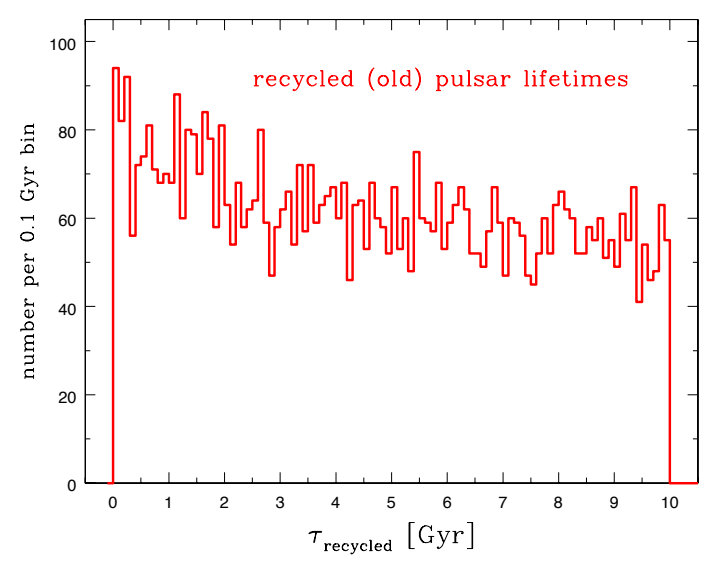


**Fig. B.2.** Recycled (old) pulsar lifetime distribution. Note that the pulsar lifetimes are distributed rather uniformly in a very broad range ( $t_{\text{recycled}} = 0$ –10 Gyr). The average lifetime is  $t_{\text{recycled,ave}} = 4.7$  Gyr, while median is  $t_{\text{recycled,med}} = 4.6$  Gyr.

NS-NS systems. However, these recycled pulsars in NS-NS systems have different spin period and magnetic field distributions compared to normal radio pulsars. Consequently, based on the observed pulsars in NS-NS systems, we adopt a uniform spin period distribution in the range 20 ms  $\langle P_s \rangle < 30$  ms and a lognormal magnetic field distribution with mean  $\langle \log_{10} B(G) \rangle = 9.5$  and standard deviation  $\sigma_{\log_{10} B} = 1$  (Lorimer 2008). As opposed to normal radio pulsars, the Parkes Multibeam survey has only detected four recycled pulsars in NS-NS systems (Manchester et al. 2005). Thus, to account for this small number of detections, we repeat the process described above multiple times to ensure that there is no significant variation in the final lifetime distribution. The representative lifetime distribution for one these simulations is shown in Fig. B.2.

#### References

```
Abbott, B. P., Abbott, R., Abbott, T. D., et al. 2017a, Phys. Rev. Lett., 119,
Abbott, B. P., Abbott, R., Abbott, T. D., et al. 2017b, ApJ, 848, L12
Anderson, S. B., Gorham, P. W., Kulkarni, S. R., Prince, T. A., & Wolszczan, A.
   1990, Nature, 346, 42
```

Bates, S. D., Lorimer, D. R., Rane, A., & Swiggum, J. 2014, MNRAS, 439, 2893 Belczynski, K., Askar, A., Arca-Sedda, M., et al. 2018, A&A, 615, A91

Belczynski, K., Bulik, T., Fryer, C. L., et al. 2010a, ApJ, 714, 1217 Belczynski, K., Dominik, M., Bulik, T., et al. 2010b, ApJ, 715, L138

Belczynski, K., Heger, A., Gladysz, W., et al. 2016a, A&A, 594, A97 Belczynski, K., Holz, D. E., Bulik, T., & O'Shaughnessy, R. 2016b, Nature, 534,

Belczynski, K., Kalogera, V., & Bulik, T. 2002, ApJ, 572, 407

Belczynski, K., Kalogera, V., Rasio, F. A., et al. 2008, ApJS, 174, 223

Belczynski, K., Klencki, J., Meynet, G., et al. 2017, ArXiv e-prints [arXiv:1706.07053]

Belczynski, K., Taam, R. E., Kalogera, V., Rasio, F. A., & Bulik, T. 2007, ApJ, 662, 504

Belczynski, K., Wiktorowicz, G., Fryer, C. L., Holz, D. E., & Kalogera, V. 2012, ApJ, 757, 91

Blanchard, P. K., Berger, E., Fong, W., et al. 2017, ApJ, 848, L22

Bray, J. C. & Eldridge, J. J. 2018, MNRAS, 480, 5657

Breton, R. P., Kaspi, V. M., Kramer, M., et al. 2008, Science, 321, 104

Cameron, A. D., Champion, D. J., Kramer, M., et al. 2018, MNRAS, 475, L57 Champion, D. J., Lorimer, D. R., McLaughlin, M. A., et al. 2004, MNRAS, 350, L61

Chen, K. & Ruderman, M. 1993, ApJ, 402, 264

Chruslinska, M., Belczynski, K., Klencki, J., & Benacquista, M. 2018, MNRAS, 474, 2937

Conselice, C. J., Wilkinson, A., Duncan, K., & Mortlock, A. 2016, ApJ, 830, 83 Corongiu, A., Kramer, M., Stappers, B. W., et al. 2007, A&A, 462, 703

de Mink, S. E. & Belczynski, K. 2015, ApJ, 814, 58

Dominik, M., Belczynski, K., Fryer, C., et al. 2012, ApJ, 759, 52 Eldridge, J. J., Stanway, E. R., & Tang, P. N. P. N. 2018, MN-RAS[arXiv:1807.07659]

Eldridge, J. J., Stanway, E. R., Xiao, L., et al. 2017, PASA, 34, e058

Faulkner, A. J., Kramer, M., Lyne, A. G., et al. 2005, ApJ, 618, L119

Ferdman, R. D. & PALFA Collaboration. 2018, in IAU Symposium, Vol. 337, Pulsar Astrophysics the Next Fifty Years, ed. P. Weltevrede, B. B. P. Perera, L. L. Preston, & S. Sanidas, 146–149

Ferdman, R. D., Stairs, I. H., Kramer, M., et al. 2013, ApJ, 767, 85

Ferdman, R. D., Stairs, I. H., Kramer, M., et al. 2014, MNRAS, 443, 2183

Fong, W., Berger, E., Chornock, R., et al. 2013, ApJ, 769, 56

Fonseca, E., Stairs, I. H., & Thorsett, S. E. 2014, ApJ, 787, 82

Fryer, C. L., Belczynski, K., Wiktorowicz, G., et al. 2012, ApJ, 749, 91

Gallazzi, A., Charlot, S., Brinchmann, J., & White, S. D. M. 2006, MNRAS, 370, 1106

Hobbs, G., Lorimer, D. R., Lyne, A. G., & Kramer, M. 2005, MNRAS, 360, 974 Hulse, R. A. & Taylor, J. H. 1975, ApJ, 195, L51

Jacoby, B. A., Cameron, P. B., Jenet, F. A., et al. 2006, ApJ, 644, L113

Janssen, G. H., Stappers, B. W., Kramer, M., et al. 2008, A&A, 490, 753

Keith, M. J., Kramer, M., Lyne, A. G., et al. 2009, MNRAS, 393, 623

Kramer, M., Stairs, I. H., Manchester, R. N., et al. 2006, Science, 314, 97

Kruckow, M. U., Tauris, T. M., Langer, N., Kramer, M., & Izzard, R. G. 2018, ArXiv e-prints [arXiv:1801.05433]

Lazarus, P., Freire, P. C. C., Allen, B., et al. 2016, ApJ, 831, 150

Licquia, T. C. & Newman, J. A. 2015, ApJ, 806, 96

Lorimer, D. R. 2008, Living Reviews in Relativity, 11 [arXiv:0811.0762]

Lorimer, D. R., Stairs, I. H., Freire, P. C., et al. 2006, ApJ, 640, 428 Lynch, R. S., Freire, P. C. C., Ransom, S. M., & Jacoby, B. A. 2012, ApJ, 745,

Madau, P. & Dickinson, M. 2014, ARA&A, 52, 415

Manchester, R. N., Hobbs, G. B., Teoh, A., & Hobbs, M. 2005, AJ, 129, 1993 Mapelli, M. & Giacobbo, N. 2018, MNRAS, 479, 4391

Martinez, J. G., Stovall, K., Freire, P. C. C., et al. 2015, ApJ, 812, 143

Martinez, J. G., Stovall, K., Freire, P. C. C., et al. 2017, ApJ, 851, L29

Ng, C., Champion, D. J., Bailes, M., et al. 2015, MNRAS, 450, 2922

Ng, C., Kruckow, M. U., Tauris, T. M., et al. 2018, MNRAS, 476, 4315

O'Shaughnessy, R., Belczynski, K., & Kalogera, V. 2008a, ApJ, 675, 566

O'Shaughnessy, R., Kalogera, V., & Belczynski, K. 2010, ApJ, 716, 615

O'Shaughnessy, R., Kim, C., Kalogera, V., & Belczynski, K. 2008b, ApJ, 672,

Palmese, A., Hartley, W., Tarsitano, F., et al. 2017, ApJ, 849, L34

Pavlovskii, K., Ivanova, N., Belczynski, K., & Van, K. X. 2017, MNRAS, 465,

Peters, P. C. 1964, Physical Review, 136, 1224

Pol, N., McLaughlin, M., & Lorimer, D. R. 2018, arXiv e-prints [arXiv:1811.04086]

Sana, H., de Mink, S. E., de Koter, A., et al. 2012, Science, 337, 444 Snyder, G. F., Torrey, P., Lotz, J. M., et al. 2015, MNRAS, 454, 1886 Stovall, K., Freire, P. C. C., Chatterjee, S., et al. 2018, ApJ, 854, L22 Swiggum, J. K., Rosen, R., McLaughlin, M. A., et al. 2015, ApJ, 805, 156 The LIGO Scientific Collaboration & the Virgo Collaboration. 2018, arXiv eprints, arXiv:1811.12907

Troja, E., Piro, L., van Eerten, H., et al. 2017, Nature, 551, 71 Troja, E., Ryan, G., Piro, L., et al. 2018, ArXiv e-prints [arXiv:1806.10624] van Leeuwen, J., Kasian, L., Stairs, I. H., et al. 2015, ApJ, 798, 118 Vigna-Gómez, A., Neijssel, C. J., Stevenson, S., et al. 2018, MNRAS, 481, 4009 Vink, J. S., de Koter, A., & Lamers, H. J. G. L. M. 2001, A&A, 369, 574 Vogelsberger, M., Genel, S., Springel, V., et al. 2014, MNRAS, 444, 1518 Webbink, R. F. 1984, ApJ, 277, 355 Weisberg, J. M., Nice, D. J., & Taylor, J. H. 2010, ApJ, 722, 1030

Woosley, S. E., Blinnikov, S., & Heger, A. 2007, Nature, 450, 390 Xu, X.-J. & Li, X.-D. 2010, ApJ, 722, 1985